Comparison of Three-Dimensional Flexible Beam Elements for Dynamic Analysis: Classical Finite Element Formulation and Absolute Nodal Coordinate Formulation

A. L. Schwab[1]
Laboratory for Engineering Mechanics,
Delft University of Technology,
Mekelweg 2,
NL-2628 CD Delft, The Netherlands
e-mail: a.l.schwab@tudelft.nl

J. P. Meijaard
Laboratory of Mechanical Automation and
Mechatronics,
Faculty of Engineering Technology,
University of Twente,
P.O. Box 217,
NL-7500 AE Enschede, The Netherlands
e-mail: j.p.meijaard@utwente.nl

Three formulations for a flexible spatial beam element for dynamic analysis are compared: a Timoshenko beam with large displacements and rotations, a fully parametrized element according to the absolute nodal coordinate formulation (ANCF), and an ANCF element based on an elastic line approach. In the last formulation, the shear locking of the antisymmetric bending mode is avoided by the application of either the two-field Hellinger–Reissner or the three-field Hu–Washizu variational principle. The comparison is made by means of linear static deflection and eigenfrequency analyses on stylized problems. It is shown that the ANCF fully parametrized element yields too large torsional and flexural rigidities, and shear locking effectively suppresses the antisymmetric bending mode. The presented ANCF formulation with the elastic line approach resolves most of these problems. [DOI: 10.1115/1.4000320]

1 Introduction

Several finite element method (FEM) formulations for spatial finite beam elements for use in multibody system dynamic programs can be found in literature. A common approach is using a small displacement formulation with respect to a reference frame moving with the average overall motion of the beam [1,2]. In order to reduce the number of degrees of freedom, a limited number of modes for the deformation are chosen [3]. The linear contribution to the stiffness matrix due to nominal or actual stresses can be included by adding a geometric stiffness matrix [4].

A different way to describe the motion of the elements is by using nodal coordinates that describe the configuration of the elements with respect to an inertial reference frame. This approach is more in line with traditional nonlinear finite element formulations used in statics. A convenient element formulation was developed by Van der Werff and Jonker [5], implemented in the program SPACAR [6] and further extended thereafter [7–9]. This formulation defines a number of generalized deformations for each element that are invariant under proper Euclidean displacements, so arbitrary rigid-body motions can exactly be described.

A description with independently interpolated displacements and rotations was given by Simo and Vu-Quoc [10]. Reduced numerical integration was used to prevent shear and membrane locking. Extensions to higher-order interpolations and physical nonlinearities can easily be included.

More recently, another approach using nodal coordinates, the absolute nodal coordinate formulation (ANCF), was proposed by Shabana [11]. This finite element formulation describes the position of a material point within the element by interpolations based on the Cartesian absolute coordinates of the nodal points and on gradients of the positions with respect to material coordinates describing a reference configuration. The use of gradients allows the exact representation of the inertia parameters of the beam as a rigid body and avoids redundancy of rotational parameters. At the cost of an increased complexity of the stiffness, the resulting element mass matrix is constant, which allows an efficient evaluation of the accelerations [12].

Poisson locking in the continuum mechanics formulation of the ANCF, which results in an overestimate of the flexural rigidity, and a poor description of the deflection of a cantilever beam were noted in Ref. [13]. An elastic line model with a reduced shear stiffness was introduced to improve the beam element. Two other approaches to improve on the description of varying bending moments in the element were proposed in Ref. [14]. In the first, terms were added to the displacement interpolation and in the second, an elastic line model was used, which cannot describe torsion and can be used to model cables. An elastic line model with constraints on the deformation of the cross section was developed in Ref. [15], which approximates classical beam models.

The purpose of the present paper, which elaborates on Ref. [16], is to make a comparison between the finite element formulation for a two-noded spatial beam element as described in Ref. [7] and several corresponding absolute nodal coordinate formulations. In order to overcome the deficiencies of the continuum mechanics formulation [17] and the elastic line formulation [18], a modification of the latter is taken into the comparison that includes deformations of the beam cross section and uncouples the shear deformation and antisymmetric bending by means of the Hellinger–Reissner [19] or Hu–Washizu [20] variational principle.

All discussed beam elements can be used for multibody system problems in which large rigid-body motions and small or large elastic vibrations need to be modeled. The ANCF element was especially developed for the large vibration problems. However, a first requirement is that problems with small vibrations can be accurately calculated. Therefore, for the comparison of the element formulations with each other and analytic solutions, only linearized eigenfrequencies and linearized static deflections for a single beam are considered.
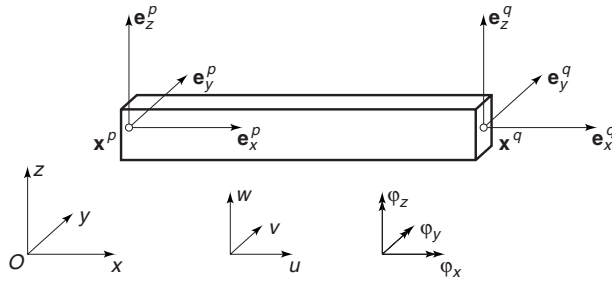

Fig. 1 FEM beam

The organization of the paper is as follows. After this introduction, a beam element based on the Timoshenko beam with large displacements and large rotations is described. Then the ANCF elements with their modifications are described. Next, results on the eigenfrequencies and deflections due to a static load for a single beam element are presented and discussed. The article ends with conclusions.

2 Classical FEM Beam Element

The finite beam element in the multibody dynamics program SPACAR is a shear flexible beam based on the elastic line concept. This supposes that the beam is slender and the cross section is doubly symmetric. Large displacements and rotations are allowed, but the deformations must remain small. The presentation of the element mainly follows [7].

The configuration of the element (Fig. 1) is determined by the positions and orientations of the two end nodes, by which it can be coupled to and interact with other elements. The positions of the end nodes p and q are given by their coordinates $\mathbf{x}^p$ and $\mathbf{x}^q$ in a global inertial system $Oxyz$. The change in orientation of a node with respect to the reference orientation is determined by an orthogonal rotation matrix $\mathbf{R}(\boldsymbol{\vartheta})$, which can be parametrized by a choice of parameters, denoted by $\boldsymbol{\vartheta}$, such as Euler angles, modified Euler angles, Rodrigues parameters, and Euler parameters. We use Euler parameters with a constraint, but this choice is immaterial to the description of the properties of the element. For a beam element, orthogonal triads of unit vectors $(\mathbf{e}_x^p, \mathbf{e}_y^p, \mathbf{e}_z^p)$ and $(\mathbf{e}_x^q, \mathbf{e}_y^q, \mathbf{e}_z^q)$ rigidly attached to the nodes p and q, respectively, are defined.

The unit vector $\mathbf{e}_x$ is perpendicular to the average warped cross-sectional plane of the beam in the sense of Cowper [21], and $\mathbf{e}_y$ and $\mathbf{e}_z$ are in the principal directions of the cross section. In the absence of shear deformations, $\mathbf{e}_x$ is tangent to the elastic line of the beam. The change in orientation of the triads is determined by the rotation matrix as

$$\mathbf{e} = \mathbf{R}(\boldsymbol{\vartheta})\bar{\mathbf{e}} \qquad (1)$$

where $\bar{\mathbf{e}}$ is a unit vector in the reference configuration.

2.1 Elastic Forces. The elastic forces are derived with the elastic line concept. The element has 6 degrees of freedom as a rigid body, while the nodes have 12 degrees of freedom. Hence the deformation that is determined by the end nodes of the element can be described by six independent generalized strains, which are functions of the positions and orientations of the nodes and the geometric parameters of the element. With $\mathbf{l} = \mathbf{x}^q - \mathbf{x}^p$ and l the length of the initial undeformed beam, we define the six generalized strains as

$$\varepsilon_1 = \sqrt{\mathbf{l}^T \mathbf{l}} - l \quad \text{(elongation)}$$

$$\varepsilon_2 = l(\mathbf{e}_z^{pT} \mathbf{e}_y^q - \mathbf{e}_y^{pT} \mathbf{e}_z^q)/2 \quad \text{(torsion)}$$

$$\varepsilon_3 = -\mathbf{l}^T \mathbf{e}_z^p, \quad \varepsilon_4 = \mathbf{l}^T \mathbf{e}_z^q \quad \text{(bending in the } xz\text{-plane)}$$

$$\varepsilon_5 = \mathbf{l}^T \mathbf{e}_y^p, \quad \varepsilon_6 = -\mathbf{l}^T \mathbf{e}_y^q \quad \text{(bending in the } xy\text{-plane)} \qquad (2)$$

These generalized strains, which may be compared with what Argyris called natural modes [22], are invariant under arbitrary rigid-body motions, so they truly measure the amount of strain in the element. If we group the positions and orientations of the nodes in a vector $\mathbf{x} = (\mathbf{x}^p, \boldsymbol{\vartheta}^p, \mathbf{x}^q, \boldsymbol{\vartheta}^q)$ and denote the vector of generalized deformations by $\boldsymbol{\varepsilon}$, then we can write for generalized strains (2) symbolically

$$\varepsilon_i = D_i(x_k), \quad i = 1, \ldots, 6, \quad k = 1, \ldots, 12 \qquad (3)$$

The energetically dual quantities of the generalized strains $\boldsymbol{\varepsilon}$ are the generalized stresses $\boldsymbol{\sigma}$. The physical meaning of these stresses is found by equating the internal virtual work of the elastic forces $\boldsymbol{\sigma}^T \delta\boldsymbol{\varepsilon}$ to the external virtual work $\mathbf{f}^T \delta\mathbf{x}$ of the nodal forces. Substitution of the virtual generalized strains derived from Eq. (3) results in

$$\sigma_i \delta\varepsilon_i = \sigma_i D_{i,k} \delta x_k = f_k \delta x_k, \quad \forall \; \delta x_k \qquad (4)$$

with the virtual nodal displacements and rotations $\delta\mathbf{x}^T = (\delta\mathbf{x}^{pT}, \delta\boldsymbol{\vartheta}^{pT}, \delta\mathbf{x}^{qT}, \delta\boldsymbol{\vartheta}^{qT})$, and a subscript after the comma to denote partial derivatives. From Eq. (4) we derive the force equilibrium conditions for the element as

$$f_k = D_{i,k} \sigma_i \qquad (5)$$

In the case of small deformations, the generalized stresses have a clear physical meaning. As the deformed and undeformed geometries are nearly the same, we consider the undeformed situation in which the beam central axis coincides with the global x-axis. For the rotational parameters $\boldsymbol{\vartheta}$ we choose the small rotations about the three coordinate axes φ_x, φ_y, and φ_z. The Jacobian of the generalized strains then takes the values

$$D_{i,k}^0 = \begin{pmatrix} -1 & 0 & 0 & 0 & 0 & 0 & 1 & 0 & 0 & 0 & 0 & 0 \\ 0 & 0 & 0 & -l & 0 & 0 & 0 & 0 & 0 & l & 0 & 0 \\ 0 & 0 & 1 & 0 & -l & 0 & 0 & 0 & -1 & 0 & 0 & 0 \\ 0 & 0 & -1 & 0 & 0 & 0 & 0 & 0 & 1 & 0 & l & 0 \\ 0 & -1 & 0 & 0 & 0 & -l & 0 & 1 & 0 & 0 & 0 & 0 \\ 0 & 1 & 0 & 0 & 0 & 0 & 0 & -1 & 0 & 0 & 0 & l \end{pmatrix}$$

$$(6)$$

The equilibrium nodal force system according to Eq. (5) is then given by

$$\mathbf{f}^p = (-\sigma_1, \sigma_6 - \sigma_5, \sigma_3 - \sigma_4), \quad \mathbf{M}^p = (-\sigma_2 l, -\sigma_3 l, -\sigma_5 l)$$

$$\mathbf{f}^q = (\sigma_1, \sigma_5 - \sigma_6, \sigma_4 - \sigma_3), \quad \mathbf{M}^q = (\sigma_2 l, \sigma_4 l, \sigma_6 l) \qquad (7)$$

From this result we interpret that σ_1 is the normal force, $\sigma_2 l$ is the torsion moment, and $\sigma_3 l$, $\sigma_4 l$, $\sigma_5 l$, and $\sigma_6 l$ are the bending moments at the nodes p and q.

If for each beam element the strains remain small by dividing the overall beam in sufficiently many elements, then the usual linear stress-strain relation can be applied, which results for the generalized stresses and strains in

$$\sigma_i = S_{ij} \varepsilon_j, \quad i, j = 1, \ldots, 6 \qquad (8)$$

where the stiffness $S_{ij} = \text{diag}(S_1, S_2, \mathbf{S}_3, \mathbf{S}_4)$ is given by

$$S_1 = EA/l, \quad S_2 = S_t/l^3$$

$$\mathbf{S}_3 = \frac{EI_y}{(1+\Phi_z)l^3}\begin{pmatrix} 4+\Phi_z & -2+\Phi_z \\ \text{symm.} & 4+\Phi_z \end{pmatrix}, \quad \Phi_z = \frac{12EI_y}{GAk_z l^2}$$

$$\mathbf{S}_4 = \frac{EI_z}{(1+\Phi_y)l^3}\begin{pmatrix} 4+\Phi_y & -2+\Phi_y \\ \text{symm.} & 4+\Phi_y \end{pmatrix}, \quad \Phi_y = \frac{12EI_z}{GAk_y l^2} \qquad (9)$$

Here, E is the modulus of elasticity (Young's modulus), G is the shear modulus, A is the area of the cross section, S_t is the torsional stiffness, I_y and I_z are the area moments of inertia of the cross

section with respect to the principal axes, and k_y and k_z are the shear coefficients according to Cowper [21]. Note that the inclusion of the shear deformation is done by a slightly modified stiffness matrix [23]. This tying of the shear deformation to the bending by means of the statics of the beam prevents problems of shear locking.

Finally the element stiffness matrix is obtained by taking partial derivatives of the nodal forces $\mathbf{f}$ with respect to the nodal coordinates, resulting in a tangent stiffness matrix

$$\bar{K}_{ij} = D_{k,i} S_{kl} D_{l,j} + D_{k,ij} \sigma_k \tag{10}$$

which consists of two parts. The last part is the geometric stiffness matrix, which, evaluated in the undeformed and unstressed geometry, is identical to zero, and the first part is the linear stiffness matrix

$$K_{ij} = D_{k,i} S_{kl} D_{l,j} \tag{11}$$

2.2 Mass Matrix. The derivation of the consistent mass formulation for the flexible spatial beam element is based on the elastic line concept. To arrive at a Timoshenko beam the rotary inertia of the cross section will be included by a separate interpolation of the angular rates of the cross section along the elastic line.

The first part of the mass matrix is obtained by neglecting the contribution of the rotary inertia and only taking the mass distribution along the elastic line into account. The interpolation for the positions on the elastic line for finite deformation is a third-order polynomial

$$\mathbf{r}(\xi) = (1 - 3\xi^2 + 2\xi^3)\mathbf{x}^p + (\xi - 2\xi^2 + \xi^3)l\mathbf{e}_x^p + (3\xi^2 - 2\xi^3)\mathbf{x}^q$$
$$+ (-\xi^2 + \xi^3)l\mathbf{e}_x^q \tag{12}$$

where $\xi = x/l$ and $x, 0 \le x \le l$ is a material coordinate along the beam axis, and where the principal directors $\mathbf{e}_x^p$ and $\mathbf{e}_x^q$ are transformed from their initial values according to Eq. (1). The kinetic energy together with the mass matrix can be obtained from the integral

$$T_1 = \frac{1}{2} m \int_0^1 \dot{\mathbf{r}}^T \dot{\mathbf{r}} \, d\xi = \frac{1}{2} \dot{\mathbf{x}}^T \mathbf{M}_1 \dot{\mathbf{x}} \tag{13}$$

where m is the total mass of the beam. If the rotations at the nodes are parametrized by $\boldsymbol{\vartheta}^p$ and $\boldsymbol{\vartheta}^q$, this results in a mass matrix

$$\mathbf{M}_1 = \frac{m}{420} \begin{pmatrix} 156\mathbf{I} & 22l\mathbf{A} & 54\mathbf{I} & -13l\mathbf{B} \\ & 4l^2\mathbf{A}^T\mathbf{A} & 13l\mathbf{A}^T & -3l^2\mathbf{A}^T\mathbf{B} \\ & & 156\mathbf{I} & -22l\mathbf{B} \\ \text{symm.} & & & 4l^2\mathbf{B}^T\mathbf{B} \end{pmatrix} \tag{14}$$

where

$$\mathbf{A} = \partial \mathbf{e}_x^p / \partial \boldsymbol{\vartheta}^p, \quad \mathbf{B} = \partial \mathbf{e}_x^q / \partial \boldsymbol{\vartheta}^q \tag{15}$$

The inertia forces can, in general, be written as the sum of mass $\times$ accelerations + convective terms

$$\mathbf{f}_{\text{in}} = -(\mathbf{M}(\mathbf{x})\ddot{\mathbf{x}} + \mathbf{h}(\mathbf{x}, \dot{\mathbf{x}})) \tag{16}$$

These convective terms $\mathbf{h}$, which are quadratic in the speeds, arise only for a nonconstant mass matrix and can be derived from the mass matrix as

$$h_i = \left(\frac{\partial M_{ij}}{\partial x_k} - \frac{1}{2} \frac{\partial M_{jk}}{\partial x_i} \right) \dot{x}_j \dot{x}_k \tag{17}$$

Clearly the mass matrix $\mathbf{M}_1$ is not constant and the corresponding convective terms are

$$\mathbf{h}_1 = \frac{m}{420} \begin{pmatrix} l(22\dot{\mathbf{A}}\dot{\boldsymbol{\vartheta}}^p - 13\dot{\mathbf{B}}\dot{\boldsymbol{\vartheta}}^q) \\ l^2\mathbf{A}^T(4\dot{\mathbf{A}}\dot{\boldsymbol{\vartheta}}^p - 3\dot{\mathbf{B}}\dot{\boldsymbol{\vartheta}}^q) \\ l(13\dot{\mathbf{A}}\dot{\boldsymbol{\vartheta}}^p - 22\dot{\mathbf{B}}\dot{\boldsymbol{\vartheta}}^q) \\ l^2\mathbf{B}^T(-3\dot{\mathbf{A}}\dot{\boldsymbol{\vartheta}}^p + 4\dot{\mathbf{B}}\dot{\boldsymbol{\vartheta}}^q) \end{pmatrix} \tag{18}$$

where

$$\dot{\mathbf{A}} = (\partial \mathbf{A}/\partial \boldsymbol{\vartheta}^p)\dot{\boldsymbol{\vartheta}}^p, \quad \dot{\mathbf{B}} = (\partial \mathbf{B}/\partial \boldsymbol{\vartheta}^q)\dot{\boldsymbol{\vartheta}}^q \tag{19}$$

The second part of the mass matrix takes into account the rotary inertia of the cross section. Interpolation of angular rates along the elastic line is more convenient than interpolation of the orientation of the cross section. The angular rates, expressed in a body-fixed reference frame, are interpolated linearly as

$$\boldsymbol{\omega}(\xi) = (1 - \xi)\boldsymbol{\omega}^p + \xi\boldsymbol{\omega}^q \tag{20}$$

where $\boldsymbol{\omega}^p$ and $\boldsymbol{\omega}^q$ are the angular rates at nodes p and q expressed in a body-fixed reference frame. The mass matrix can be obtained from the kinetic energy integral

$$T_2 = \frac{1}{2} \int_{\xi=0}^{\xi=1} \boldsymbol{\omega}^T d\mathbf{J}\boldsymbol{\omega} = \frac{1}{2} \dot{\mathbf{x}}^T \mathbf{M}_2 \dot{\mathbf{x}} \tag{21}$$

where $d\mathbf{J}$ is the mass moment of inertia matrix along the body-fixed axes of an infinitesimal small section of length $l\,d\xi$. The body-fixed angular rates at the nodes expressed in terms of the nodal rotational parameters $\boldsymbol{\vartheta}^p$ and $\boldsymbol{\vartheta}^q$ are

$$\boldsymbol{\omega}^p = \mathbf{P}(\boldsymbol{\vartheta}^p)\dot{\boldsymbol{\vartheta}}^p, \quad \boldsymbol{\omega}^q = \mathbf{Q}(\boldsymbol{\vartheta}^q)\dot{\boldsymbol{\vartheta}}^q \tag{22}$$

where the matrices $\mathbf{P}$ and $\mathbf{Q}$ have the same functional dependence on the rotation parameters. For a constant cross section with a sectional mass moment of inertia matrix $d\mathbf{J} = m\bar{\mathbf{J}} d\xi$, the second part of the mass matrix, which takes into account the rotary inertia of the cross section, is

$$\mathbf{M}_2 = \frac{m}{6} \begin{pmatrix} \mathbf{0} & \mathbf{0} & \mathbf{0} & \mathbf{0} \\ & 2\mathbf{P}^T\bar{\mathbf{J}}\mathbf{P} & \mathbf{0} & \mathbf{P}^T\bar{\mathbf{J}}\mathbf{Q} \\ & & \mathbf{0} & \mathbf{0} \\ \text{symm.} & & & 2\mathbf{Q}^T\bar{\mathbf{J}}\mathbf{Q} \end{pmatrix} \tag{23}$$

where the corresponding convective terms $\mathbf{h}_2$ can be derived from this mass matrix by application of Eq. (17). For slender beams the rotary inertia contributions are usually small compared with the regular inertia terms. If the principal dimension of the cross section is h, then $\bar{\mathbf{J}}$ is of the order h^2 and the rotary inertia contributions are of the order $(h/l)^2$ compared with the regular inertia terms (14) and (18). Therefore the linear interpolation in Eq. (20) is sufficiently accurate.

3 ANCF Beam

In this section a spatial beam element with two nodes according to the absolute nodal coordinate formulation will be presented. In the first part we follow mainly the description by Yakoub and Shabana [17] and Shabana and Yakoub [18].

A distinguishing point in the ANCF is the use of slope vectors to describe the orientation of the cross section in the nodes, where the slope vectors are not necessarily unit vectors. This leaves more room for the cross section to deform and change shape. It is expected [17,18] that this type of description, together with a three-dimensional continuum mechanics approach, leads to more accurate results. A well-known major advantage of this description is that it leads to a constant mass matrix. Unfortunately, the expressions for the elastic forces are more complex.

The configuration of the beam element (Fig. 2) is determined by the position and slope vectors of the two end nodes p and q. Each node is defined by one vector for the position $\mathbf{r}$ and three
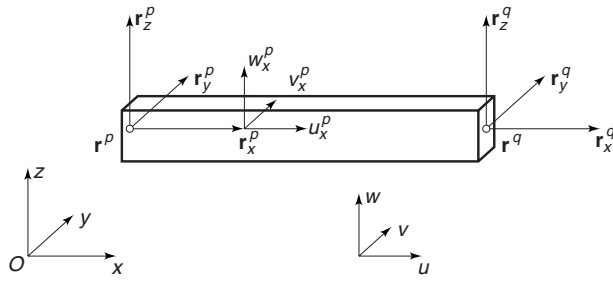
Fig. 2 ANCF beam

vectors for the slopes $\mathbf{r}_x$, $\mathbf{r}_y$, and $\mathbf{r}_z$, where every vector is expressed in a global inertial system $Oxyz$. Thus the element has 24 nodal coordinates given by the vector

$$\mathbf{e} = (\mathbf{r}^{pT}, \mathbf{r}_x^{pT}, \mathbf{r}_y^{pT}, \mathbf{r}_z^{pT}, \mathbf{r}^{qT}, \mathbf{r}_x^{qT}, \mathbf{r}_y^{qT}, \mathbf{r}_z^{qT})^T \tag{24}$$

The location of an arbitrary point $\mathbf{r}$ in the beam is determined by the interpolation

$$\mathbf{r} = \mathbf{S}(x,y,z)\mathbf{e} \tag{25}$$

where $\mathbf{S}$ is the element shape function and $\mathbf{e}$ is the vector of nodal coordinates. The shape function is obtained using polynomials that are in this case cubic in x and linear in y and z, where x is a material coordinate along the beam axis and y and z are the two other perpendicular directions. The element shape function matrix $\mathbf{S}$ is now defined as

$$\mathbf{S} = (S_1\mathbf{I}, S_2\mathbf{I}, S_3\mathbf{I}, S_4\mathbf{I}, S_5\mathbf{I}, S_6\mathbf{I}, S_7\mathbf{I}, S_8\mathbf{I}) \tag{26}$$

where $\mathbf{I}$ is the 3×3 identity matrix and the polynomials

$$S_1 = 1 - 3\xi^2 + 2\xi^3, \quad S_2 = l(\xi - 2\xi^2 + \xi^3)$$

$$S_3 = l(1-\xi)\eta, \quad S_4 = l(1-\xi)\zeta$$

$$S_5 = 3\xi^2 - 2\xi^3, \quad S_6 = l(-\xi^2 + \xi^3)$$

$$S_7 = l\xi\eta, \quad S_8 = l\xi\zeta \tag{27}$$

with the nondimensional coordinates

$$\xi = x/l, \quad \eta = y/l, \quad \zeta = z/l \tag{28}$$

and l the initial length of the beam. The initial undeformed configuration where the beam central axis coincides with the global x-axis is

$$\mathbf{r}|_0 = \mathbf{S}\mathbf{e}|_0 \tag{29}$$

with the initial nodal coordinates $\mathbf{e}|_0$ as

$$\mathbf{e}|_0 = (0^T, \mathbf{e}_x^T, \mathbf{e}_y^T, \mathbf{e}_z^T, l\mathbf{e}_x^T, \mathbf{e}_x^T, \mathbf{e}_y^T, \mathbf{e}_z^T)^T \tag{30}$$

with fixed triads $(\mathbf{e}_x, \mathbf{e}_y, \mathbf{e}_z)$ of the global inertial system $Oxyz$. Indeed, substitution of $\mathbf{e}|_0$ in Eq. (29) leads to the identities $\mathbf{r}|_0 = (x, y, z)^T$.

3.1 Elastic Forces, Fully Parametrized Element. The elastic forces are derived from a general continuum mechanics approach. We start from the displacements $\mathbf{u}$ of an arbitrary point of the beam expressed in the global $Oxyz$ coordinate system as given by

$$\mathbf{u} = \mathbf{r} - \mathbf{r}|_0 \tag{31}$$

Substitution of these displacements in the Green–Lagrange strain tensor

$$\varepsilon_{ij} = \tfrac{1}{2}(u_{i,j} + u_{j,i} + u_{k,i}u_{k,j}), \quad i,j,k = x,\dots,z \tag{32}$$

where partial derivatives are denoted by $u_{x,y} = \partial u_x / \partial y$, etc., leads to the strain tensor expressed in the absolute coordinates $\mathbf{r}$ and their derivatives as

$$\varepsilon_{ij} = \frac{1}{2}(r_{k,i}r_{k,j} - \delta_{ij}) = \frac{1}{2}\begin{pmatrix} \mathbf{r}_{,x}^T\mathbf{r}_{,x} - 1 & \mathbf{r}_{,x}^T\mathbf{r}_{,y} & \mathbf{r}_{,x}^T\mathbf{r}_{,z} \\ & \mathbf{r}_{,y}^T\mathbf{r}_{,y} - 1 & \mathbf{r}_{,y}^T\mathbf{r}_{,z} \\ \text{symm.} & & \mathbf{r}_{,z}^T\mathbf{r}_{,z} - 1 \end{pmatrix} \tag{33}$$

From this we identify six independent strain components, which we write in the form of a strain vector $\boldsymbol{\epsilon}$ such that the vector dot product $\frac{1}{2}\boldsymbol{\sigma}^T\boldsymbol{\epsilon}$ represents the elastic energy. The components of the strain vector are now

$$\epsilon_1 = \tfrac{1}{2}(\mathbf{r}_{,x}^T\mathbf{r}_{,x} - 1), \quad \epsilon_4 = \mathbf{r}_{,x}^T\mathbf{r}_{,y}$$

$$\epsilon_2 = \tfrac{1}{2}(\mathbf{r}_{,y}^T\mathbf{r}_{,y} - 1), \quad \epsilon_5 = \mathbf{r}_{,y}^T\mathbf{r}_{,z}$$

$$\epsilon_3 = \tfrac{1}{2}(\mathbf{r}_{,z}^T\mathbf{r}_{,z} - 1), \quad \epsilon_6 = \mathbf{r}_{,z}^T\mathbf{r}_{,x} \tag{34}$$

and the energetically dual stress vector components are the three normal stresses σ_1, σ_2, and σ_3, and the three shear stresses σ_4, σ_5, and σ_6. The virtual work of the elastic stresses now can be written as

$$\delta W = \int_V \boldsymbol{\sigma}^T \delta\boldsymbol{\epsilon}\, dV \tag{35}$$

Under the assumption of a Saint-Venant–Kirchhoff material model, a homogeneous isotropic elastic material, the stress vector $\boldsymbol{\sigma}$ is related to the strain vector as

$$\boldsymbol{\sigma} = \mathbf{E}\boldsymbol{\epsilon} \tag{36}$$

where the nonzero elastic coefficients $\mathbf{E}$ are given by

$$E_{ij} = \frac{2G}{(1-2\nu)}\begin{pmatrix} 1-\nu & \nu & \nu \\ \nu & 1-\nu & \nu \\ \nu & \nu & 1-\nu \end{pmatrix}, \quad i,j = 1,\dots,3$$

$$E_{kk} = G, \quad k = 4,\dots,6 \tag{37}$$

Here, G is the shear modulus and ν is Poisson's ratio. Equating the virtual work of the elastic stresses with the virtual work of the external nodal forces $\mathbf{Q}$ as in

$$\int_V \boldsymbol{\sigma}^T \delta\boldsymbol{\epsilon}\, dV = \mathbf{Q}^T \delta\mathbf{e} \tag{38}$$

yields the elastic nodal forces expressed in terms of the nodal displacements

$$\mathbf{Q} = \int_V (\partial\boldsymbol{\epsilon}/\partial\mathbf{e})^T \mathbf{E}\boldsymbol{\epsilon}\, dV \tag{39}$$

The tangent stiffness matrix is obtained by linearizing the elastic forces with respect to the nodal displacements

$$\overline{\mathbf{K}} = \int_V (\partial\boldsymbol{\epsilon}/\partial\mathbf{e})^T \mathbf{E}(\partial\boldsymbol{\epsilon}/\partial\mathbf{e})\, dV + \int_V (\partial^2\boldsymbol{\epsilon}/\partial\mathbf{e}^2)^T \mathbf{E}\boldsymbol{\epsilon}\, dV \tag{40}$$

The second matrix is the geometric stiffness matrix, which, evaluated in the undeformed and unstressed geometry, is identical to zero, whereas the first matrix is the linear stiffness matrix

$$\mathbf{K} = \int_V (\partial\boldsymbol{\epsilon}/\partial\mathbf{e})^T \mathbf{E}(\partial\boldsymbol{\epsilon}/\partial\mathbf{e})\, dV \tag{41}$$

Finally, we will evaluate the linear stiffness matrix in the undeformed configuration. With the notion that the slopes in the initially undeformed configuration are identical to the global directions

$$\mathbf{r}_{,x}|_0 = \mathbf{e}_x, \quad \mathbf{r}_{,y}|_0 = \mathbf{e}_y, \quad \mathbf{r}_{,z}|_0 = \mathbf{e}_z \tag{42}$$

and

$$\left.\frac{\partial \mathbf{r}_{,x}}{\partial \mathbf{e}}\right|_0 = \mathbf{S}_{,x}, \qquad \left.\frac{\partial \mathbf{r}_{,y}}{\partial \mathbf{e}}\right|_0 = \mathbf{S}_{,y}, \qquad \left.\frac{\partial \mathbf{r}_{,z}}{\partial \mathbf{e}}\right|_0 = \mathbf{S}_{,z} \qquad (43)$$

the partial derivatives of the strain vector evaluated at this initial undeformed configuration become

$$\left.\frac{\partial \boldsymbol{\epsilon}}{\partial \mathbf{e}}\right|_0 = \begin{pmatrix} \mathbf{S}_{1,x} \\ \mathbf{S}_{2,y} \\ \mathbf{S}_{3,z} \\ \mathbf{S}_{1,y} + \mathbf{S}_{2,x} \\ \mathbf{S}_{2,z} + \mathbf{S}_{3,y} \\ \mathbf{S}_{3,x} + \mathbf{S}_{1,z} \end{pmatrix} \qquad (44)$$

where $\mathbf{S}_{i,j}$ stands for the ith row of $\mathbf{S}_{,j}$. Substitution into Eq. (41) and evaluating the integral over the volume of the beam lead to the desired linear stiffness matrix

$$\mathbf{K}^0 = \int_V (\partial \boldsymbol{\epsilon}/\partial \mathbf{e})|_0^T \mathbf{E} (\partial \boldsymbol{\epsilon}/\partial \mathbf{e})|_0 \mathrm{d}V \qquad (45)$$

3.2 Mass Matrix. The absolute nodal coordinate formulation leads to inertia forces that can be expressed as minus the product of a constant mass matrix times the accelerations of the nodal coordinates. There are no inertia forces that are quadratic in the velocities. The constant mass matrix is defined as

$$\mathbf{M} = \int_V \rho \mathbf{S}^T \mathbf{S} \mathrm{d}V \qquad (46)$$

The above integral defines a mass matrix that only depends on the mass distribution and the dimensions of the beam and, under the assumption of a consistent shape function, captures all linear and rotary inertia effects.

3.3 Elastic Forces, Elastic Line Approach. The fully parametrized beam element of Sec. 3.1 suffers from shear locking for antisymmetric bending, as will be shown in Sec. 4. As an alternative, we propose to develop an element in which the elastic line concept is used, along lines as in Ref. [18]. For the interpolation of points of the beam we will still use the same cubic form in the longitudinal direction and linear form in the transverse direction as in the fully parametrized element (25) and (26), but all deformations (extension, shear, torsion, and bending) will be evaluated on the elastic line.

First we define the slopes on the elastic line as

$$\mathbf{r}_x = \mathbf{r}_{,x}(x,0,0), \quad \mathbf{r}_y = \mathbf{r}_{,y}(x,0,0), \quad \mathbf{r}_z = \mathbf{r}_{,z}(x,0,0) \qquad (47)$$

With these slopes we define nine generalized deformations

$$\varepsilon_x = \tfrac{1}{2}(\mathbf{r}_x^T \mathbf{r}_x - 1), \quad \varepsilon_y = \tfrac{1}{2}(\mathbf{r}_y^T \mathbf{r}_y - 1), \quad \varepsilon_z = \tfrac{1}{2}(\mathbf{r}_z^T \mathbf{r}_z - 1)$$

$$\gamma_{yz} = \mathbf{r}_y^T \mathbf{r}_z \quad \gamma_{xy} = \mathbf{r}_x^T \mathbf{r}_y, \quad \gamma_{xz} = \mathbf{r}_x^T \mathbf{r}_z$$

$$\kappa_x = \tfrac{1}{2}(\mathbf{r}_z^T \mathbf{r}_y' - \mathbf{r}_y^T \mathbf{r}_z'), \quad \kappa_y = -\mathbf{r}_z^T \mathbf{r}_x', \quad \kappa_z = \mathbf{r}_y^T \mathbf{r}_x' \qquad (48)$$

where a prime denotes a derivative with respect to x. The first six deformations are the usual Green–Lagrange strains: the first four, ε_x, ε_y, and ε_z, and γ_{yz}, represent the extension of the beam and the deformation of the cross section, and γ_{xy} and γ_{xz} are the transverse shear deformations. For small strains, κ_x represents the torsion, and κ_y and κ_z the bending deformations. Definitions of the bending deformations better in agreement with Timoshenko's beam theory are $\kappa_y = \mathbf{r}_x^T \mathbf{r}_z'$ and $\kappa_z = -\mathbf{r}_x^T \mathbf{r}_y'$, but these are not used, because they would lead to constant curvature for small deformations, instead of a linear variation for the definition in Eq. (48), and prevent antisymmetric bending altogether.

The strain energy of the beam can be written as the sum of four

distinct parts, as in $W^e = W_l + W_t + W_b + W_s$. The individual strain energies are for extension and coupled deformation of the cross section

$$W_l = \frac{1}{2} l \int_0^1 (A \bar{\varepsilon}_i E_{ij} \bar{\varepsilon}_j) \mathrm{d}\xi, \quad i,j = 1, \dots, 4 \qquad (49)$$

with the strains $\bar{\varepsilon}_i = (\varepsilon_x, \varepsilon_y, \varepsilon_z, \gamma_{yz})$ and the elasticity coefficients E_{ij} as in Eq. (37); for torsion and bending

$$W_t = \frac{1}{2} l \int_0^1 (S_t \kappa_x^2) \mathrm{d}\xi, \quad W_b = \frac{1}{2} l \int_0^1 (EI_y \kappa_y^2 + EI_z \kappa_z^2) \mathrm{d}\xi \qquad (50)$$

and for the transverse shear deformation

$$W_s = \frac{1}{2} l \int_0^1 (GAk_y \gamma_{xy}^2 + GAk_z \gamma_{xz}^2) \mathrm{d}\xi \qquad (51)$$

The elastic forces are determined, in the same manner as in Sec. 3.1, from equating the variation of the elastic energy to the virtual work of the nodal forces

$$\delta W^e = (\partial W^e / \partial \mathbf{e}) \delta \mathbf{e} = \mathbf{Q}^{eT} \delta \mathbf{e} \qquad (52)$$

Then the linear stiffness matrix is found by linearizing the elastic forces with respect to the nodal coordinates at the undeformed reference configuration

$$\mathbf{K} = (\partial \mathbf{Q}^e / \partial \mathbf{e})|_0 \qquad (53)$$

Because the elastic energy is a direct sum of contributions due to extension, torsion, bending, and shear, the same holds for the stiffness matrix. The individual contributions to the stiffness matrix are as follows: For the extension

$$\mathbf{K}_l = l \int_0^1 (\bar{\varepsilon}_{i,\mathbf{e}})|_0^T E_{ij} (\bar{\varepsilon}_{j,\mathbf{e}})|_0 A \mathrm{d}\xi, \quad i,j = 1, \dots, 4 \qquad (54)$$

for the torsion

$$\mathbf{K}_t = l \int_0^1 S_t (\kappa_{x,\mathbf{e}})|_0^T (\kappa_{x,\mathbf{e}})|_0 \mathrm{d}\xi \qquad (55)$$

for the bending

$$\mathbf{K}_b = l \int_0^1 EI_y (\kappa_{y,\mathbf{e}})|_0^T (\kappa_{y,\mathbf{e}})|_0 \mathrm{d}\xi + l \int_0^1 EI_z (\kappa_{z,\mathbf{e}})|_0^T (\kappa_{z,\mathbf{e}})|_0 \mathrm{d}\xi$$

$$(56)$$

and for the shear deformation

$$\mathbf{K}_s = l \int_0^1 GAk_y (\gamma_{xy,\mathbf{e}})|_0^T (\gamma_{xy,\mathbf{e}})|_0 \mathrm{d}\xi + l \int_0^1 GAk_z (\gamma_{xz,\mathbf{e}})|_0^T (\gamma_{xz,\mathbf{e}})|_0 \mathrm{d}\xi$$

$$(57)$$

resulting in a total linear stiffness matrix

$$\mathbf{K} = \mathbf{K}_l + \mathbf{K}_t + \mathbf{K}_b + \mathbf{K}_s \qquad (58)$$

The partial derivatives of the generalized strains with respect to the nodal coordinates in the initially undeformed configuration take on even simpler forms as in Eqs. (42) and (44) since the only variable is now the elastic line coordinate x.

With the cubic/linear interpolation on the elastic line according to Eqs. (26) and (47), adding the contribution of the shear deformation according to Eq. (51) will result in shear locking for antisymmetric bending, as will be shown in Sec. 4. Therefore we propose to add the transverse shear stiffness by means of a variational principle in which we are free to define not only the position field but also the deformation field or the stress distribution.

3.3.1 Hellinger–Reissner approach. In the Hellinger–Reissner [19] variational approach we are free to define both the position

field and the stress distribution. The strain field is related to the stress field by the constitutive relation. This can be advantageous if the stress distribution, usually from an engineering point of view, is known beforehand. The general form of this principle is

$$\delta \int_V [\boldsymbol{\sigma}^T \boldsymbol{\varepsilon}(\mathbf{r}) - W_c(\boldsymbol{\sigma})] dV - \mathbf{Q} \delta \mathbf{r} = 0 \qquad (59)$$

where $\boldsymbol{\varepsilon}(\mathbf{r})$ is the strain as calculated from the position field and $W_c(\boldsymbol{\sigma})$ is the complementary elastic energy density, while $\mathbf{Q}$ contains all external forces and inertia forces.

To resolve the shear locking problem we consider the case of pure shear deformation. We assume that the shear forces will vary linearly over the elastic line of the element. The strain energy of the shear deformation is the sum of the shear in the y- and the z-direction. For the shear forces in the z-direction we assume a linear shear stress distribution according to

$$\tau_{xz} = \mathbf{N} \boldsymbol{\tau}_z^* \qquad (60)$$

with the shape function

$$\mathbf{N} = (1 - \xi, \xi) \qquad (61)$$

and the shear stresses at the nodes

$$\boldsymbol{\tau}_z^* = (\tau_{xz}^p, \tau_{xz}^q)^T \qquad (62)$$

The Hellinger–Reissner shear strain functional is now

$$W_{sz}^* = \int_V (\boldsymbol{\tau}_{xz}^T \gamma_{xz} - W_c(\tau_{xz})) dV \qquad (63)$$

where W_c is the complementary shear stress energy according to

$$W_c(\tau_{xz}) = \frac{1}{2Gk_z} \tau_{xz}^2 \qquad (64)$$

with shear factor k_z to account for the fact that the shear stress is not uniformly distributed over the cross section [21]. Substitution of the linear shear stress distribution from Eq. (60) results in the shear strain functional

$$W_{sz}^* = \int_V \left(\boldsymbol{\tau}_z^{*T} \mathbf{N}^T \gamma_{xz} - \frac{1}{2Gk_z} \boldsymbol{\tau}_z^{*T} \mathbf{N}^T \mathbf{N} \boldsymbol{\tau}_z^* \right) dV \qquad (65)$$

with the shear strain distribution γ_{xz} according to Eq. (48). For this shear strain functional we seek a stationary value with respect to the generalized shear stress parameters $\boldsymbol{\tau}^*$, resulting in

$$\delta W_{sz}^* = \int_V \delta \boldsymbol{\tau}_z^{*T} \left(\mathbf{N}^T \gamma_{xz} - \frac{1}{Gk_z} \mathbf{N}^T \mathbf{N} \boldsymbol{\tau}_z^* \right) dV = 0 \qquad (66)$$

Integration over the volume yields

$$\mathbf{W}_{xz} - \frac{Al}{Gk_z} \mathbf{H} \boldsymbol{\tau}_z^* = \mathbf{0} \qquad (67)$$

with the shear strain terms

$$\mathbf{W}_{xz}(\mathbf{e}) = Al \int_0^1 (\mathbf{N}^T \gamma_{xz}(\mathbf{e})) d\xi \qquad (68)$$

which are in general nonlinear functions in the nodal coordinates $\mathbf{e}$, and the constant coefficient matrix

$$\mathbf{H} = \begin{pmatrix} 1/3 & 1/6 \\ 1/6 & 1/3 \end{pmatrix} \qquad (69)$$

From this we can solve for the generalized shear stress parameters

$$\boldsymbol{\tau}_z^* = \mathbf{S}_z \mathbf{W}_{xz}, \quad \mathbf{S}_z = \frac{Gk_z}{Al} \mathbf{H}^{-1} = \frac{Gk_z}{Al} \begin{pmatrix} 4 & -2 \\ -2 & 4 \end{pmatrix} \qquad (70)$$

Substitution in the original shear energy function yields the shear energy according to the Hellinger–Reissner principle

$$W_{sz}^* = \frac{1}{2} \mathbf{W}_{xz}^T \mathbf{S}_z \mathbf{W}_{xz} \qquad (71)$$

The shear strain energy for shear forces in the y-direction W_{sy}^* can be derived in the same manner resulting in a total shear strain energy function of

$$W_s^* = \frac{1}{2} \mathbf{W}_{xy}^T \mathbf{S}_y \mathbf{W}_{xy} + \frac{1}{2} \mathbf{W}_{xz}^T \mathbf{S}_z \mathbf{W}_{xz} \qquad (72)$$

The strain energy for the beam with the adapted shear stiffness according to the Hellinger–Reissner principle now becomes

$$W^{e*} = W_l + W_s^* + W_t + W_b \qquad (73)$$

The shear stiffness matrix according to the Hellinger–Reissner principle, which replaces Eq. (57), is found in the same manner as in Eq. (53) resulting in

$$\mathbf{K}_s^* = (\mathbf{W}_{xy,\mathbf{e}})|_0^T \mathbf{S}_y (\mathbf{W}_{xy,\mathbf{e}})|_0 + (\mathbf{W}_{xz,\mathbf{e}})|_0^T \mathbf{S}_z (\mathbf{W}_{xz,\mathbf{e}})|_0 \qquad (74)$$

3.3.2 Hu–Washizu Approach. The shear locking problem can be resolved even more when one has a greater freedom in choosing the various interpolations. In the Hu–Washizu variational approach [24] we are free to define not only the position field $\mathbf{r}$ and the stress field $\boldsymbol{\sigma}$ but also the strain field $\boldsymbol{\varepsilon}$. The general form of this principle is

$$\delta \int_V [W(\boldsymbol{\varepsilon}) + \boldsymbol{\sigma}^T (\boldsymbol{\varepsilon}(\mathbf{r}) - \boldsymbol{\varepsilon})] dV - \mathbf{Q} \delta \mathbf{r} = 0 \qquad (75)$$

where $\boldsymbol{\varepsilon}(\mathbf{r})$ is the strain as calculated from the position field and $W(\boldsymbol{\varepsilon})$ is the elastic potential energy density, while $\mathbf{Q}$ contains all external forces and inertia forces. The variation has to be taken for the stress field, the strain field, and the position field. The weak solution is found for arbitrary admissible variations of the stress field $\delta \boldsymbol{\sigma}$, strain field $\delta \boldsymbol{\varepsilon}$, and position field $\delta \mathbf{r}$. When one takes the strain field in accordance with the stress field one regains the Hellinger–Reissner principle.

For the shear deformation in the z-direction, we have $\boldsymbol{\sigma} = \tau_{xz}$, $\boldsymbol{\varepsilon} = \gamma_{xz}$, and $\mathbf{r}$ is as in Eq. (25). In the case of pure shear deformation we assume that the shear strain will vary linearly over the elastic line of the element

$$\gamma_{xz} = \mathbf{N} \boldsymbol{\gamma}_z^* \qquad (76)$$

with the shape function $\mathbf{N}$ from Eq. (61) and the shear strains at the nodes

$$\boldsymbol{\gamma}_z^* = (\gamma_{xz}^p, \gamma_{xz}^q)^T \qquad (77)$$

The elastic shear strain energy is

$$W_{sz} = \frac{1}{2} \int_V Gk_z \gamma_{xz}^2 dV \qquad (78)$$

Take for the stress field two Dirac functions, one at each end of the beam, which means that the kinematic conditions are only enforced at both ends. With the Dirac or impulse function $\hat{\delta}(\xi)$ the stress field then becomes

$$\tau_{xz} = \mathbf{I} \boldsymbol{\tau}_z^* \qquad (79)$$

with the impulse shape function

$$\mathbf{I} = (\hat{\delta}(0), \hat{\delta}(1)) \qquad (80)$$

and the shear stresses at the nodes

$$\boldsymbol{\tau}_z^* = (\tau_{xz}^p, \tau_{xz}^q)^T \qquad (81)$$

For the strain $\boldsymbol{\varepsilon}(\mathbf{r})$ as calculated from the position field we use the expression for the shear strain on the elastic line $\mathbf{r}_x^T \mathbf{r}_z$ from Eq. (48). Then, variation of the stresses gives the kinematic conditions, namely, that the shear strains at the nodes are determined by

$$\boldsymbol{\gamma}_z^* = ((\mathbf{r}_x^T \mathbf{r}_z)|_{\xi=0}, (\mathbf{r}_x^T \mathbf{r}_z)|_{\xi=1}) \qquad (82)$$

Next, variation of the shear strains gives the constitutive behavior, which, after integration over the volume, results in

$$\boldsymbol{\tau}_z^* = GAk_z l \mathbf{H} \boldsymbol{\gamma}_z^* \qquad (83)$$

The variation of the position field, which in this case finally comes down to the variation of the nodal coordinates $\mathbf{e}$, results in the element equilibrium equations

$$\mathbf{Q} = \left(\frac{\partial \boldsymbol{\gamma}_z^*}{\partial \mathbf{e}} \right)^T \boldsymbol{\tau}_z^* \qquad (84)$$

Substitutions of Eq. (82) in Eq. (83) and of Eq. (83) in Eq. (84) give the nodal elastic shear forces $\mathbf{Q}_{sz}^e$ in terms of the nodal coordinates. The linear shear stiffness matrix, which replaces Eq. (57), is found in the same manner as in Eq. (53), resulting for the shear in the z-direction in

$$K_{sz}^{**} = GAk_z l \left(\frac{\partial \boldsymbol{\gamma}_z^*}{\partial \mathbf{e}} \right)\Big|_0^T \mathbf{H} \left(\frac{\partial \boldsymbol{\gamma}_z^*}{\partial \mathbf{e}} \right)\Big|_0 \qquad (85)$$

The contribution of the shear in the y-direction to the linear shear stiffness matrix is found in the same manner as above.

4 Results and Discussion

To investigate the performance of the three different element types, classical FEM, ANCF fully parametrized, and ANCF with an elastic line approach and a Hellinger–Reissner or a Hu–Washizu variational method, a number of tests on linear problems have been performed. The first is a static loading on a cantilevered beam. Since the ultimate goal for these elements is the use in a multibody dynamics environment, an eigenfrequency analysis on a beam with various boundary conditions has been performed as a second test. Moreover, the eigenfrequency analysis yields coordinate-free results and therefore makes a comparison easy and objective.

The beam is modeled by one finite element and has an undeformed length l and a uniform square cross section of width and height $h=0.02l$. The material is isotropic and linearly elastic with modulus of elasticity E, Poisson's ratio ν, and volumetric mass density ρ. The solutions depend on Poisson's ratio, and throughout a value of $\nu=0.3$ is used. The shear factors for a square cross section are $k_y=k_z=10(1+\nu)/(12+11\nu)$ [21]. The torsional stiffness is given by $S_t=Gk_xI_p$, with $G=E/(2(1+\nu))$, the shear distribution factor $k_x=0.8436$ [25], and the polar area moment of inertia $I_p=I_y+I_z$. The beam is initially aligned along the x-axis with the principal axes of the cross section along the y-axis and z-axis.

For the static test a cantilevered beam loaded at the tip by a bending moment M_y and a transverse force F_z is considered. The boundary conditions for the classical FEM element are straightforward: All three displacements and three rotations at node p are suppressed. For the ANCF elements the three displacements of node p are suppressed together with all three displacements of the two cross-sectional slope vectors $\mathbf{r}_y$ and $\mathbf{r}_z$ in node p. This is as if the cross section is welded on all sides to the support. The generalized applied forces $\mathbf{Q}_e$ for the ANCF element associated with the nodal coordinates $\mathbf{e}$ due to the applied bending moment M_y and transverse forces F_z can be found by a virtual work approach. It is assumed that stress distributions $\sigma_x(y,z)$ and $\tau_{xz}(y,z)$ in the cross section are such that the only nonzero static result is a moment about the y-axis as in $M_y=\int z\sigma_x dA$ and a transverse force $F_z=\int \tau_{xz} dA$. For instance, a linear normal stress $\sigma_x=c_1 z$ and a constant shear stress $\tau_{xz}=c_2$ will do. Then the virtual work of these stresses in the cross section must be equal to the virtual work of the applied generalized force $\mathbf{Q}_e$ as in

Table 1 Dimensionless transverse tip displacement $\bar{w}$, cross-sectional rotation $\bar{\varphi}_{\text{csy}}$, and elastic line rotation $\bar{\varphi}_{\text{ely}}$ for a cantilevered beam of length l loaded by a moment M_y at the tip for four different element types: classical FEM, ANCF fully parametrized, ANCF with a Hellinger–Reissner variational method, and ANCF with a Hu–Washizu variational method. Displacements are nondimensionalized by $M_y l^2/(EI_y)$ and rotations by $M_y l/(EI_y)$. The shear factor $\Phi_z=12EI_y/(GAk_z l^2)$ and a common factor $\Psi=(1-2\nu)(1+\nu)/(1-\nu)$ are used.

Method	$\bar{w}$	$\bar{\varphi}_{\text{csy}}$	$\bar{\varphi}_{\text{ely}}$
Classical FEM	$-\frac{1}{2}$	1	1
ANCF-fp	$-\frac{1}{2}\Psi$	Ψ	Ψ
ANCF-HR	$-\frac{1}{2}-\frac{1}{2}\Phi_z$	$1+\Phi_z$	$1+\frac{1}{2}\Phi_z$
ANCF-HW	$-\frac{1}{2}-\frac{1}{2}\Phi_z$	$1+\Phi_z$	$1+\frac{1}{2}\Phi_z$

$$\delta W = \int (\delta r_x \sigma_x + \delta r_z \tau_{xz}) dA = \mathbf{Q}_e^T \delta\mathbf{e} \qquad (86)$$

where the virtual displacements in the cross section $\delta\mathbf{r} = (\delta r_x, \delta r_y, \delta r_z)$ are interpolated according to Eq. (25). This results in an external generalized force in node q as

$$\mathbf{Q}_e^q = (0,0,F_z,0,0,0,0,0,0,M_y,0,0) \qquad (87)$$

Clearly, the rotation of the cross section about the y-axis is determined by the x-displacement of the slope vector $\mathbf{r}_z$.

The transverse tip displacement w and the rotations at the tip about the y-axis of the cross section φ_{csy} and of the elastic line φ_{ely} resulting from the static tests are presented in Tables 1 and 2. Note that the two rotations differ due to transverse shear deformation. For the classical FEM element they are defined as $\varphi_{\text{csy}}=\varphi_y$ and $\varphi_{\text{ely}}=-\partial w/\partial x$ and for the ANCF element as $\varphi_{\text{csy}}=(r_z)_x$ and $\varphi_{\text{ely}}=-(r_x)_z$. The classical FEM element yields the exact solution for both loading cases. The ANCF fully parametrized element shows, for the moment loading Table 1, in all results an offset by a Poisson factor $\Psi=(1-2\nu)(1+\nu)/(1-\nu)$. This is so, because the anticlastic deformation of the cross section cannot be described by the continuum position field. This Poisson factor is also present in the results for the transverse force loading, Table 2, but here the leading term in the displacement is also off by a factor of $\frac{3}{4}$, which is due to the shear locking. The effect of transverse shear is present but off by a factor k_z since the transverse shear stress distribution is not taken into account with the ANCF fully parametrized element approach. The elastic line approach together with a Hellinger–Reissner variational method gives some improvement in that the Poisson factor is gone but the element still suffers from a poor prediction of the deflection. This is due to the weak inclusion of the connection between the deflection of the center line and the shear deformation at the clamped end, and some additional transverse shear, $O(h/l)^2$, which is present in all solutions. Application of the Hu–Washizu variational principle yields better

Table 2 Dimensionless transverse tip displacement $\bar{w}$, cross-sectional rotation $\bar{\varphi}_{\text{csy}}$, and elastic line rotation $\bar{\varphi}_{\text{ely}}$ as in Table 1 but now for loading by a transverse force F_z. Displacements are nondimensionalized by $F_z l^3/(EI_y)$ and rotations by $F_z l^2/(EI_y)$.

Method	$\bar{w}$	$\bar{\varphi}_{\text{csy}}$	$\bar{\varphi}_{\text{ely}}$
Classical FEM	$\frac{1}{3}+\frac{1}{12}\Phi_z$	$-\frac{1}{2}$	$-\frac{1}{2}-\frac{1}{12}\Phi_z$
ANCF-fp	$\frac{1}{4}\Psi+\frac{1}{12}k_z\Phi_z$	$-\frac{1}{2}\Psi$	$-\frac{1}{2}\Psi-\frac{1}{12}k_z\Phi_z$
ANCF-HR	$\frac{1}{4}+\frac{1}{3}\Phi_z$	$-\frac{1}{2}-\frac{1}{2}\Phi_z$	$-\frac{1}{2}-\frac{1}{3}\Phi_z$
ANCF-HW	$\frac{1}{3}+\frac{1}{3}\Phi_z$	$-\frac{1}{2}-\frac{1}{2}\Phi_z$	$-\frac{1}{2}-\frac{1}{3}\Phi_z$

Table 3 Dimensionless eigenfrequencies $\Omega = \omega/\omega_{B,T,L}$ for the free vibration of a completely free beam modeled by one element for four different element types: classical FEM, ANCF fully parametrized, ANCF elastic line approach with a Hellinger–Reissner variational principle, and ANCF elastic line approach with a Hu–Washizu variational method together with the analytical solution for an Euler–Bernoulli beam. The eigenfrequencies are nondimensionalized by $\omega_B = \sqrt{EI/(\rho A l^4)}$ for bending modes, $\omega_T = \sqrt{G/(\rho l^2)}$ for torsion mode, and $\omega_L = \sqrt{E/(\rho l^2)}$ for longitudinal (**Lg**) and cross-sectional (**Cs**) modes.

Mode	Analytic	Classical FEM	ANCF-fp	ANCF-HR	ANCF-HW
B 1st(2)	22.3733	26.8060	31.0797	26.8060	26.8060
B 2nd(2)	61.6728	90.0950	1270.38	91.6088	90.1501
T	2.8855	3.1817	3.4641	3.1817	3.1817
Lg 1st	3.1416	2.8697	3.2201	3.2201	3.2201
Lg 2nd	6.2832	–	7.7447	7.7446	7.7446
Lg 3rd	9.4248	–	14.7666	14.7666	14.7666
Cs 1,2	–	–	107.489	99.081	99.114
Cs 3,4	–	–	107.600	99.114	100.684
Cs 5,6	–	–	151.911	151.911	151.911
Cs 7,8	–	–	151.926	151.911	151.911
Cs 9	–	–	240.221	240.221	240.221
Cs 10	–	–	240.245	240.236	240.236

results. The leading term in the transverse displacement at the tip for a transverse force loading is now correct, because the shear deformations at the nodes are used to calculate the contribution in the stiffness matrix due to shear. The transverse shear correction shows an offset by a factor of 4. For the constant moment loading the solution still suffers form spurious transverse shear deformation.

The dynamic tests are eigenfrequency analyses on a beam modeled by one element with various boundary conditions. The first case is a fully free beam, which is somewhat idealized but has a number of advantages: There are no kinematic boundary conditions and it demonstrates the possibility of the element to describe the six rigid-body motions. The nonzero dimensionless eigenfrequencies for the various elements are presented in Table 3 together with the analytic solution for an Euler–Bernoulli beam. The zero eigenvalues are not reported since all element types describe the rigid-body modes exactly. Owing to the symmetric cross section some frequencies come in pairs. The first observation that we make is that the ANCF elements yield 12 further eigenfrequencies, of which 2 are longitudinal modes and 10 are cross-sectional modes with a high frequency. These cross-sectional modes are depicted in Fig. 3, where the aspect ratio of the cross section versus the beam length is exaggerated for a better illustration of the modes. The first bending mode in the ANCF fully parametrized is too high by a factor $\sqrt{(1-\nu)/(1+\nu)/(1-2\nu)} \approx 1.16$, which is expected because the anticlastic deformation of the cross section cannot be described by the continuum position field. Note that this result is also present in the dynamic response of the midpoint deflection of the pendulum beam from Fig. 8 in Ref. [17]. The torsional eigenfrequency is also too high, because the factor k_x is not included. The ANCF fully parametrized element gives a large value for the second bending mode, because this mode is coupled to a transverse shearing deformation, a phenomenon that is referred to as shear locking. The modified ANCF with the elastic line approach gives a far more realistic value. This second bending mode for all ANCF elements is illustrated in Fig. 4. The shear locking is evident in the fully parametrized element. The elastic line approach with the Hellinger–Reissner method yields a correct eigenfrequency but incorrect rotations of the cross section at the nodes. The Hu–Washizu method yields not only a correct eigenfrequency but also correct rotations of the cross section at the nodes. Note that the rotations between the nodes along the elastic line are incorrect. All ANCF elements give identical and good approximations for the longitudinal eigenfrequencies, because the interpolation is cubic instead of linear, as for the classical FEM element.

The second boundary condition case is a simply supported beam. The boundary conditions for the classical FEM beam are straightforward. Both nodes are supported in the yz-plane and in node p the horizontal displacement and the rotation along the central axis are suppressed. This leaves six degrees of freedom, namely,

$$\mathbf{u}^c = (\varphi_y^p, \varphi_z^p, u^q, \varphi_x^q, \varphi_y^q, \varphi_z^p) \qquad (88)$$

where the displacements of a position vector $\mathbf{r}^p$ are denoted by (u^p, v^p, w^p). For the ANCF element we apply the same boundary conditions, where the rotation along the central axis in node p is
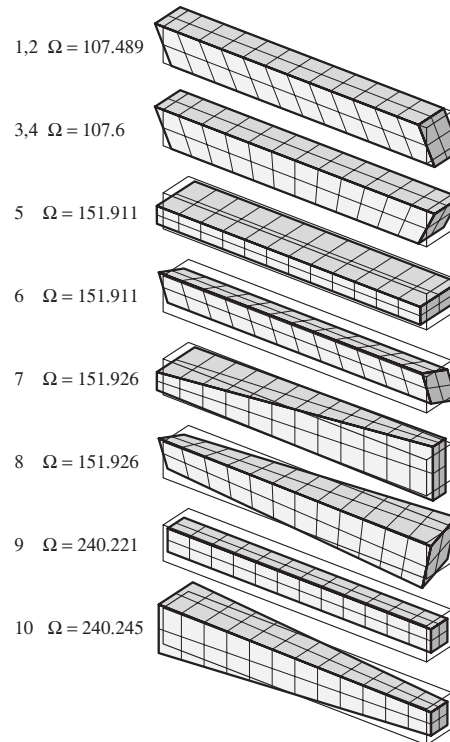

1,2 $\Omega = 107.489$

3,4 $\Omega = 107.6$

5 $\Omega = 151.911$

6 $\Omega = 151.911$

7 $\Omega = 151.926$

8 $\Omega = 151.926$

9 $\Omega = 240.221$

10 $\Omega = 240.245$

Fig. 3 The ten cross-sectional eigenmodes together with their dimensionless eigenfrequencies Ω for the free vibration of a completely free beam modeled by one ANCF fully parametrized element. See also Table 3.
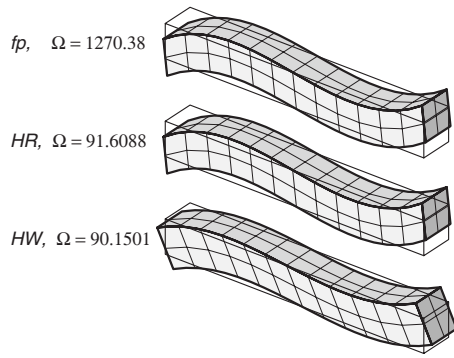
Fig. 4 The second bending eigenmode together with the dimensionless eigenfrequency Ω for the free vibration of a completely free beam modeled by one element for three ANCF element types: fully parametrized, elastic line approach with a Hellinger–Reissner method and elastic line approach with a Hu–Washizu method. See also Table 3.
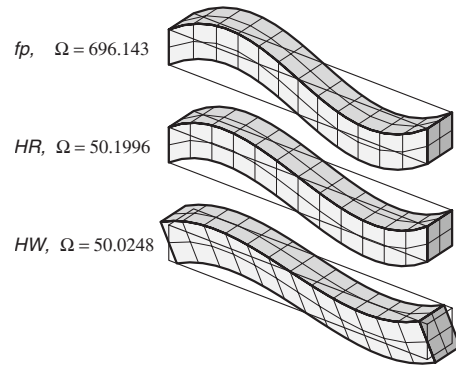

Fig. 5 The second bending eigenmode together with the dimensionless eigenfrequency Ω as in Fig. 4 but now for a simply supported beam. See also Table 4.

now suppressed by fixing the y-displacement of the z-slope vector: v_z^p. Displacements of a slope vector $\mathbf{r}_x^p$ are denoted by (u_x^p, v_x^p, w_x^p), etc. The remaining degrees of freedom, 18 in total, are

$$\mathbf{u}^c = (u_x^p, v_x^p, w_x^p, u_y^p, v_y^p, w_y^p, u_z^p, w_z^p, u^q, u_x^q, v_x^q, w_x^q, u_y^q, v_y^q, w_y^q, u_z^q, v_z^q, w_z^q)$$
(89)

The results of this analysis are presented in Table 4. The ANCF fully parametrized element shows the same drawbacks as in the previous case. The Hellinger–Reissner approach resolves the shear locking in the second bending mode but still yields incorrect cross-sectional rotations at the nodes, as can be seen in Fig. 5. The torsional and longitudinal eigenfrequencies show similar behavior as in the free-free case. Also the cross-sectional modes are nearly identical in frequency, because the boundary conditions for the simply supported beam put almost no restriction on the deformation of the cross section. This is not the case for a cantilevered beam, the third type of boundary condition considered. Here the same boundary conditions are taken as in the static test, namely, restricting all displacements of the built-in node and fixing the two slope vectors $\mathbf{r}_y^p$ and $\mathbf{r}_z^p$. The remaining degrees of freedom, 15 in total, are

$$\mathbf{u}^c = (u_x^p, v_x^p, w_x^p, u^q, v^q, w^q, u_x^q, v_x^q, w_x^q, u_y^q, v_y^q, w_y^q, u_z^q, v_z^q, w_z^q) \quad (90)$$

These results are presented in Table 5 and Figs. 6 and 7. The results for the longitudinal and torsion eigenfrequencies are as in the simply supported case. For bending, we see the same kind of phenomena as before, especially the shear locking in the second

bending mode for the ANCF fully parametrized element; see Fig. 6. The ANCF element with Hellinger–Reissner method still gives rather high values for the two bending eigenfrequencies. This can be attributed to the difficulty in prescribing the condition of zero rotation of the cross section for the clamped end. Because the Hellinger–Reissner formulation relaxes the rigidity against shear deformation, shear can still occur at the ends of the beam for asymmetric bending; the shear is only small in an average sense. The Hu–Washizu approach gives more realistic values and modes. The cross-sectional modes are now fewer, seven instead of ten, and their frequencies have shifted somewhat compared with those from the simply supported case. This is due to the restriction of the deformation of the cross section at the built-in node. This is also the reason for the relatively low eigenfrequency of the first (double) cross-sectional mode (Fig. 7) because the cross-sectional deformation is now coupled to the global displacement.

5 Conclusions

In this paper some formulations for a flexible spatial beam have been compared. In general, the classical FEM formulation gives good results for the linearized case. Some shortcomings in the spatial beam formulation given in Ref. [17] were found, especially that it yields too large torsional and flexural rigidities and that shear locking effectively suppresses the asymmetric bending mode. An ANCF element with an elastic line approach, along similar lines as in Ref. [18], has been proposed. This formulation yields better torsional and flexural rigidities. The shear locking of the asymmetric bending mode can be avoided by the aid of the Hellinger–Reissner variational principle. The problem of the

Table 4 Dimensionless eigenfrequencies Ω as in Table 3 but now for a simply supported beam

Mode	Analytic	Classical FEM	ANCF-fp	ANCF-HR	ANCF-HW
B 1st(2)	9.8696	10.9526	12.6988	10.9526	10.9526
B 2nd(2)	39.4784	49.9942	696.14	50.1996	50.0248
T	1.4427	1.5908	1.7319	1.5907	1.5907
Lg 1st	1.5708	1.6408	1.5724	1.5724	1.5724
Lg 2nd	4.7124	–	5.0546	5.0546	5.0546
Lg 3rd	7.8540	–	11.5848	11.5848	11.5848
Cs 1,2	–	–	107.417	99.015	99.031
Cs 3,4	–	–	107.510	99.031	99.361
Cs 5	–	–	107.433	107.424	107.424
Cs 6	–	–	151.911	151.911	151.911
Cs 7	–	–	151.915	151.911	151.911
Cs 8	–	–	151.926	151.911	151.911
Cs 9	–	–	240.196	240.194	240.194
Cs 10	–	–	240.238	240.231	240.231

Table 5   Dimensionless eigenfrequencies Ω as in Table 3 but now for a cantilevered beam

Mode	Analytic	Classical FEM	ANCF-fp	ANCF-HR	ANCF-HW
B 1st(2)	3.5160	3.5318	5.1860	4.4608	3.5297
B 2nd(2)	22.0345	34.7051	361.6853	59.4731	34.6532
T	1.4427	1.5908	1.7321	1.5908	1.5908
Lg 1st	1.5708	1.6408	1.7275	1.7275	1.7275
Lg 2nd	4.7124	–	5.2873	5.2872	5.2872
Lg 3rd	7.8540	–	11.6967	11.6967	11.6967
Cs 1,2	–	–	5.660	2.293	4.938
Cs 3,4	–	–	107.508	99.081	99.805
Cs 5,6	–	–	151.915	151.911	151.911
Cs 7	–	–	240.224	240.221	240.221

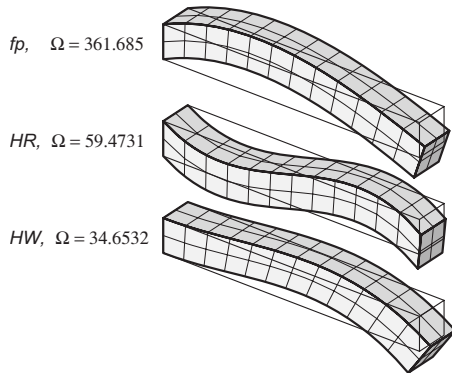fp,   Ω = 361.685

HR,   Ω = 59.4731

HW,   Ω = 34.6532

Fig. 6   The second bending eigenmode together with the dimensionless eigenfrequency Ω as in Fig. 4 but now for a cantilevered beam. See also Table 5.

fp,   Ω = 5.660

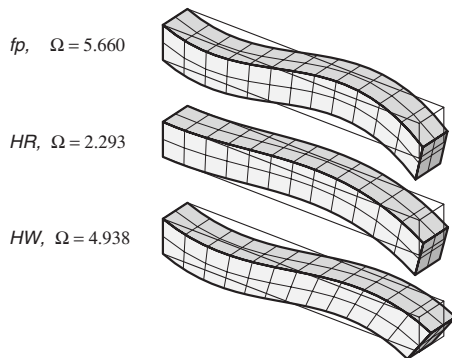HR,   Ω = 2.293

HW,   Ω = 4.938

Fig. 7   The first (double) cross-sectional eigenmode together with the dimensionless eigenfrequency Ω as in Fig. 4 but now for a cantilevered beam. See also Table 5.

proper imposition of the boundary conditions at clamped ends is alleviated by the judicious application of the Hu–Washizu variational principle.

As a direction of future research, it is desirable to develop the ANCF spatial beam based on the elastic line concept further.

Acknowledgment

References

[1] Fraeijs de Veubeke, B., 1976, "The Dynamics of Flexible Bodies," Int. J. Eng. Sci., **14**, pp. 895–913.
[2] Song, J. O., and Haug, E. J., 1980, "Dynamic Analysis of Planar Flexible Mechanisms," Comput. Methods Appl. Mech. Eng., **24**, pp. 359–381.
[3] Shabana, A., and Wehage, R. A., 1983, "Variable Degree-of-Freedom Component Mode Analysis of Inertia Variant Flexible Mechanical Systems," ASME J. Mech., Transm., Autom. Des., **105**, pp. 371–378.
[4] Wallrapp, O., and Schwertassek, R., 1991, "Representation of Geometric Stiffening in Multibody System Simulation," Int. J. Numer. Methods Eng., **32**, pp. 1833–1850.
[5] van der Werff, K., and Jonker, J. B., 1984, "Dynamics of Flexible Mechanisms," *Computer Aided Analysis and Optimization of Mechanical System Dynamics*, E. J. Haug, ed., Springer-Verlag, Berlin, pp. 381–400.
[6] Jonker, J. B., and Meijaard, J. P., 1990, "SPACAR—Computer Program for Dynamic Analysis of Flexible Spatial Mechanisms and Manipulators," *Multibody Systems Handbook*, W. O. Schiehlen, ed., Springer-Verlag, Berlin, pp. 123–143.
[7] Meijaard, J. P., 1996, "Validation of Flexible Beam Elements in Dynamics Programs," Nonlinear Dyn., **9**, pp. 21–36.
[8] Meijaard, J. P., 2001, "Some Developments in the Finite Element Modelling and Solution Techniques for Flexible Multibody Dynamical Systems," *Euroconference on Computational Mechanics and Engineering Practice*, Szczyrk, Poland, Sept. 19–21, J. Stadnicki, ed., University of Łódź, Bielsko-Biała, Poland, pp. 48–55.
[9] Schwab, A. L., 2002, "Dynamics of Flexible Multibody Systems, Small Vibrations Superimposed on a General Rigid Body Motion," Ph.D. thesis, Delft University of Technology, Delft, The Netherlands.
[10] Simo, J. C., and Vu-Quoc, L., 1986, "A Three-Dimensional Finite-Strain Rod Model. Part II: Computational Aspects," Comput. Methods Appl. Mech. Eng., **58**, pp. 79–115.
[11] Shabana, A. A., 1997, "Flexible Multibody Dynamics: Review of Past and Recent Developments," Multibody Syst. Dyn., **1**, pp. 189–222.
[12] Shabana, A. A., 1998, "Computer Implementation of the Absolute Nodal Coordinate Formulation for Flexible Multibody Dynamics," Nonlinear Dyn., **16**, pp. 293–306.
[13] Sopanen, J. T., and Mikkola, A. M., 2003, "Description of Elastic Forces in Absolute Nodal Coordinate Formulation," Nonlinear Dyn., **34**, pp. 53–74.
[14] Gerstmayr, J., and Shabana, A. A., 2006, "Analysis of Thin Beams and Cables Using the Absolute Nodal Co-Ordinate Formulation," Nonlinear Dyn., **45**, pp. 109–130.
[15] Sugiyama, H., Gerstmayr, J., and Shabana, A. A., 2006, "Deformation Modes in the Finite Element Absolute Nodal Coordinate Formulation," J. Sound Vib., **298**, pp. 1129–1149.
[16] Schwab, A. L., and Meijaard, J. P., 2005, "Comparison of Three-Dimensional Flexible Beam Elements for Dynamic Analysis: Finite Element Method and Absolute Nodal Coordinate Formulation," *Proceedings of the IDETC/CIE 2005, ASME 2005 International Design Engineering Technical Conferences and Computers and Information in Engineering Conference*, Long Beach, CA, Sept. 24–28, ASME, New York, CD-ROM.
[17] Yakoub, R. Y., and Shabana, A. A., 2001, "Three Dimensional Absolute Nodal Coordinate Formulation for Beam Elements: Implementation and Applications," ASME J. Mech. Des., **123**, pp. 614–621.
[18] Shabana, A. A., and Yakoub, R. Y., 2001, "Three Dimensional Absolute Nodal Coordinate Formulation for Beam Elements: Theory," ASME J. Mech. Des., **123**, pp. 606–613.
[19] Reissner, E., 1953, "On a Variational Theorem for Finite Elastic Deformations," J. Math. Phys., **32**, pp. 129–135.
[20] Washizu, K., 1982, *Variational Methods in Elasticity and Plasticity*, Pergamon, New York.
[21] Cowper, G. R., 1966, "The Shear Coefficient in Timoshenko's Beam Theory," ASME J. Appl. Mech., **33**, pp. 335–340.
[22] Argyris, J. H., 1966, "Continua and Discontinua, an Aperçu of Recent Developments of the Matrix Displacement Methods," *Matrix Methods in Structural Mechanics*, J. S. Przemienniecki, R. M. Bader, W. F. Bozich, J. R. Johnson, and W. J. Mykytow, eds., Wright-Patterson Air Force Base, Dayton, OH, pp. 11–189.
[23] Przemieniecki, J. S., 1968, *Theory of Matrix Structural Analysis*, McGraw-Hill, New York.
[24] Fraeijs de Veubeke, B., 1965, "Displacement and Equilibrium Models in the Finite Element Method," *Stress Analysis, Recent Developments in Numerical and Experimental Methods*, O. C. Zienkiewicz and G. S. Holister, eds., Wiley, New York, Chap. 9, pp. 145–197 [reprinted in International Journal for Numerical Methods in Engineering, **52**, 2001, pp. 287–342].
[25] Timoshenko, S. P., and Goodier, J. N., 1987, *Theory of Elasticity*, McGraw-Hill, New York.